Integration of the Vegetation Phenology Module Improves Ecohydrological Simulation by the SWAT-Carbon Model

Mingwei Li[1], Shouzhi Chen[1], Fanghua Hao[1], Nan Wang[1], Zhaofei Wu[1], Yue Xu[2], Jing Zhang[1], Yongqiang Zhang[3], Yongshuo H. Fu[1]

5 [1]College of Water Sciences, Beijing Normal University, Beijing 100875, China
[2]College of Urban and Environmental Sciences, Central China Normal University, Wuhan 430079, China
[3]Key Laboratory of Water Cycle and Related Land Surface Processes, Institute of Geographic Sciences and Natural Resources Research, Chinese Academy of Sciences, Beijing 100101, China

Correspondence to: Yongshuo H. Fu (yfu@bnu.edu.cn)

10 **Abstract.** Vegetation phenology and hydrological cycles are closely interacted from leaf and species levels to watershed and global scales. As one of the most sensitive biological indicators of climate change, plant phenology is essential to be simulated accurately in hydrological models. Despite the Soil and Water Assessment Tool (SWAT) has been widely used for estimating hydrological cycles, its lack of integration with the phenology module has led to substantial uncertainties. In this study, we developed a process-based vegetation phenology module and coupled it with the SWAT-Carbon model to 15 investigate the effects of vegetation dynamics on runoff in the upper reaches of Jinsha River watershed in China. The modified SWAT-Carbon model showed reasonable performance in phenology simulation, with root mean square error (RMSE) of 9.89 days for the start-of-season (SOS) and 7.51 days for the end-of-season (EOS). Simulations of both vegetation dynamics and runoff were also substantially improved compared to the original model. Specifically, the simulation of leaf area index significantly improved with the coefficient of determination (R^2) increased by 0.62, the Nash–20 Sutcliffe efficiency (NSE) increased by 2.45, and the absolute percent bias (PBIAS) decreased by 69.0 % on average. Additionally, daily runoff simulation also showed notably improvement, particularly noticeable in June and October, with R^2 rising by 0.22 and NSE rising by 0.43 on average. Our findings highlight the importance of integrating vegetation phenology into hydrological models to enhance modeling performance.

1 Introduction

25 Vegetation plays a crucial role as a link between the land and the atmosphere through its influence on the processes of the carbon, water, and energy cycles (Bonan, 2008; Zhou et al., 2023). Plant phenology is one of the most sensitive bioindicators of climate change (IPCC, 2021; Fu et al., 2015; Vitasse et al., 2022), closely interacting with the hydrological cycles (Chen et al., 2022a; Hwang et al., 2014; Kim et al., 2018). Therefore, vegetation phenological processes must be accurately simulated accurately in hydrological models. The Soil and Water Assessment Tool (SWAT) has been widely used to model 30 watershed hydrological characteristics (Bhatta et al., 2019; Tian et al., 2020). However, the performance of its vegetation

module and its simulation of vegetation phenology remains poor, resulting in large uncertainties in the simulation of hydrological processes (Chen et al., 2023). To improve predictions of ecohydrological processes under future climate change conditions, it is essential to modify the vegetation module by considering vegetation phenology.

In recent decades, climate change has substantially shifted vegetation phenology, with an advance in the start-of-season (SOS) (Fu et al., 2014) and a delay in the end-of-season (EOS) (Piao et al., 2019). This has contributed to the extension of the growing season by 2–10 days per decade (Zhao et al., 2015; Garonna et al., 2016; Shen et al., 2022), closely interacting with hydrological processes from leaf, species levels to watershed and global scales (Chen et al., 2022b). At the leaf scale, earlier spring leaf-out would enhance the transpiration and increase the water requirement of plants, resulting in increased water flux from the soil to the atmosphere. At the watershed scale, the extension of the growing season would reduce runoff through increased evapotranspiration (ET) (Gaertner et al., 2019; Geng et al., 2020; Kim et al., 2018). Shifting in vegetation phenology affects both the magnitude and the timing of hydrological processes (Creed et al., 2015; Hwang et al., 2023). Therefore, developing a hydrological model capable of characterizing vegetation phenology is essential for comprehensive understanding hydrological processes.

The SWAT has been extensively used to assess the impact of climate change on water processes across a variety of watershed scales. The updated SWAT-Carbon model was developed to improve performance in terms of terrestrial carbon and water cycles (Mukundan et al., 2023; Zhang et al., 2013). As in the original version, SWAT-Carbon employs a simplified version of the Environmental Policy Impact Climate (EPIC) vegetation growth module (Arnold et al., 1998), which determines SOS and EOS based on a daylength threshold calculated as a function of latitude. However, phenological processes are complex, determined not only by daylength, but also by temperature and precipitation (Piao et al., 2015; Wu et al., 2023; Peñuelas et al., 2004). For example, temperature is regarded as the dominant driver of spring phenology, with spring warming largely advancing leaf-out dates by meeting the forcing requirement earlier (Ge et al., 2015; Fu et al., 2018). However, winter warming-induced reductions in chilling accumulation would increase the forcing requirement and delay the leaf-out date (Fu et al., 2015; Wu et al., 2023). Therefore, the EPIC module cannot capture the real phenological processes (Ma et al., 2019), and coupling specific phenology module with the SWAT-Carbon model is urgently needed to accurately simulate hydrological processes.

The Tibetan Plateau has experienced seriously climate change, greatly influencing vegetation dynamics and regional water cycles (Shen et al., 2022; Li et al., 2022). In this study, utilizing a typical watershed in the Tibetan Plateau, upper reaches of the Jinsha River watershed, we first developed a process-based vegetation phenology module consisted of spring and autumn phenology models that considers both temperature and photoperiod. Subsequently, we coupled this module into the SWAT-Carbon model. The objectives of our study are as follows: 1) to develop a process-based vegetation phenology module and integrate it into the SWAT-Carbon model; 2) to elucidate the effects of vegetation phenology and climate change on

watershed ecohydrological processes; and 3) to forecast future shifts in runoff under different emission scenarios using the modified SWAT-Carbon model.

2 Materials and Methods

65 ### 2.1 Study Area

Our study focused on the upper reaches of the Jinsha River watershed in China, and the Jinsha River is located in the upper reach of the Yangtze River (Figure 1a). The elevation difference of the upper Jinsha River watershed is 4,773 m (Figure 1b), and the drainage area is 216,440 km^2. The multiyear mean temperature is approximately -2.56 ± 4.11 °C and the multiyear mean annual precipitation is approximately 467 ± 135 mm from 1982 to 2018. Influenced by monsoons, precipitation is 70 mainly observed during June–September, accounting for over 75 % of the annual total, with peak precipitation typically occurring in July. The land use types in the study area showed minimal change during 2007–2014, with grassland (61.4 %) and forest (14.6 %) representing the dominant vegetation types (Figure 1c). Grassland areas are primarily distributed in the upstream region of the basin, whereas forests are prevalent in the downstream area.
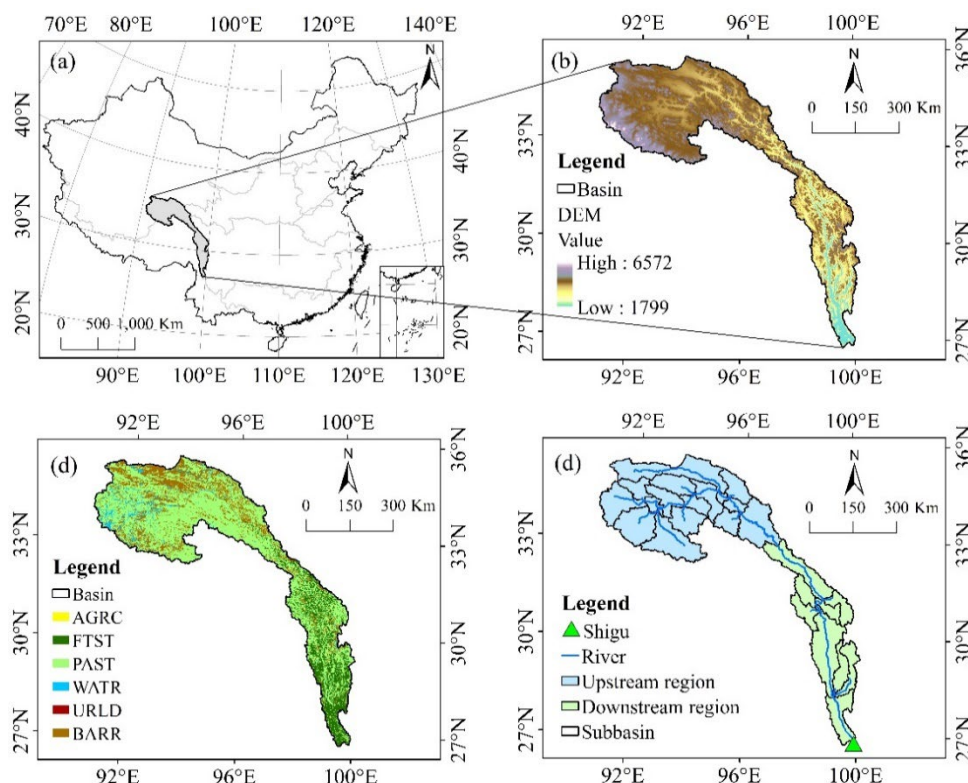
75 **Figure 1: Study area.** (a) Location of the upper Jinsha River watershed, (b) digital elevation model (DEM), (c) distribution of land use types (AGRC-farmland, FRST-forest, PAST-grassland, WATR-water, URLD- residential area, BARR-unused land), and (d) division of subbasins and the location of the Shigu hydrological gauging station.

2.2 Dataset

The sources of the datasets used for phenology models and the SWAT-Carbon model are listed in Table 1.

80 2.2.1 Digital Elevation Model (DEM), Land Use, and Soil Data

The watershed and river network of study area were delineated using a digital elevation model (DEM) with 90-m resolution (Figure 1b) in ArcSWAT2012. The watershed was first subdivided into 28 subbasins (Figure 1d) using topographic characteristics, and then discretized into 1922 hydrologic response units (HRUs) based on land use, soil data, and slope characteristics.

85 We extracted land use data with 1-km spatial resolution from the Resources and Environmental Sciences and Data Center, Institute of Geographic Sciences and Natural Resources Research, Chinese Academy of Sciences (https://www.resdc.cn/). This extracted data were reclassified to match the land use classes for HRU delineation in the SWAT model (Figure 1c). There were six classes of land use identified in the watershed: farmland (ARGC), forest (FRST), grassland (PAST), water (WATR), residential area (URLD), and unused land (BARR).

90 The soil map of the upper reaches of the Jinsha River watershed was obtained from the Food and Agriculture Organization of the United Nations (http://www.fao.org). We used the Soil Water Atmosphere Plant model (SWAP: http://hydrolab.arsusda.gov/soilwater) to develop the database of soil properties for the studied watershed.

2.2.2 Climate Data and Runoff

Because of the limited distribution of meteorological stations in the study area, gridded climate data were used as observed
95 values to force both the original and the modified SWAT-Carbon models. We used daily meteorological data from 1982 to 2018 with 0.1° spatial resolution extracted from the China Meteorological Forcing Dataset (CMFD), which included precipitation, temperature, relative humidity, wind speed, and solar radiation (He et al., 2020). This dataset was developed by the Institute of Tibetan Plateau Research under the Chinese Academy of Sciences, and it represents the optimal combination of in situ observations, satellite retrials, and meteorological reanalysis.

100 We selected four CMIP6 models, i.e., CanESM5, FGOALS-g3, MPI-ESM1-2-HR, and MRI-ESM2-0 under three emission scenarios (SSP1-2.6, SSP2-4.5 and SSP5-8.5), to predict vegetation phenology and future runoff. Daily time series of mean temperature, maximum temperature, minimum temperature, and precipitation were acquired from the CMIP6 website (https://esgf-node.llnl.gov/search/cmip6/). CMIP6 data are biased in local areas (Stevens and Bony, 2013) and therefore it is necessary to correct those errors. First, we interpolated the CMIP6 data to 0.1° spatial resolution using linear interpolation.
105 Then, the CMFD was employed as the reference to correct the bias in CMIP6 models using the empirical mapping technique

(Gudmundsson et al., 2012; Wilcke et al., 2013). Daily empirical cumulative distribution functions for the calibration period were produced using a moving window of ±15 days (Thrasher et al., 2012).

Daily runoff data (2007–2014) of the Shigu hydrological gauging station, located at the upper reaches of Jinsha River watershed outlet, were obtained from the Chinese Hydrological Data Yearbook.

110 **2.2.3 Vegetation Data**

We obtained the Global Inventory Modeling and Mapping Studies third generation normalized difference vegetation index (GIMMS3g NDVI) dataset from the Ecological Forecasting Lab (https://data.tpdc.ac.cn/en/data/9775f2b4-7370-4e5e-a537-3482c9a83d88/) for 1982–2020 (spatial resolution: 1/12°, temporal resolution: every 15 d).

Leaf area index (LAI) data from 1982 to 2018 was acquired from the Global Land Surface Satellite (GLASS) product with
115 0.05° spatial resolution and an eight-day temporal interval (http://glass-product.bnu.edu.cn). LAI time series for forest and grassland areas were obtained through area-weighted averaging of FRST and PAST grid values within the studied watershed (Strauch and Volk, 2013; Zhang et al., 2020).

Table 1: Details of the data used in this study.

Data	Source	Characteristics
Digital elevation model (DEM)	Geospatial Data Cloud (https://www.gscloud.cn/)	SRTMDEM 90M
Land use types	Center for Resources and Environmental Sciences and Data (https://www.resdc.cn/)	1 km spatial resolution
Soil map	Food and Agriculture Organization of the United Nations (http://www.fao.org)	Harmonized World Soil Database v 1.2
Observed meteorological data	China Meteorological Forcing Dataset (https://data.tpdc.ac.cn/home)	daily, 0.1° spatial resolution
Observed runoff	Chinese Hydrological Data Yearbook	Shigu hydrological gauging station, daily
Normalized difference vegetation index (NDVI)	Global Inventory Modeling and Mapping Studies third generation (GIMMS$_{3g}$) (https://data.tpdc.ac.cn/en/data/9775f2b4-7370-4e5e-a537-3482c9a83d88/)	15 d, 1/12° spatial resolution
Leaf area index data (LAI)	Global Land Surface Satellite (GLASS) product (http://glass-product.bnu.edu.cn).	8 d, 0.05° spatial resolution

2.3 SWAT-Carbon Model Modification

120   The SWAT is a comprehensive, process-oriented, and physically based/process-based semi-distributed hydrological model (Neitsch et al., 2011). The SWAT-Carbon model (https://sites.google.com/view/swat-carbon/home), as an updated vision, is developed to enhance the simulation of terrestrial carbon cycles. However, the SWAT-Carbon model still performs poorly in estimating vegetation dynamics (e.g., phenology and LAI). More realistic phenology data could enhance the performance of LAI simulation, which would further improve the accuracy of runoff simulated by the hydrological model. Therefore, we

125   developed a novel method to enhance the SWAT-Carbon model by integrating a process-based vegetation phenology module into it. This phenology module consists of two phenology models: the UniChill model for simulating SOS and the DM model for simulating EOS. These phenology models provide dynamic simulation of plant phenology to replace the exact dates of the SOS and EOS in SWAT-Carbon model without the need for any management settings in the operation schedule.

The UniChill model, proposed by Chuine (2000), hypothesizes that spring phenology is regulated both by chilling

130   temperatures and by forcing temperatures during the dormancy period. Because of the certain range of chilling and forcing temperatures, we added temperature conditions when calculating the state of the chilling and forcing phases (Fu et al., 2012). The chilling phase starts at the onset of dormancy (t_0, fixed to 1 September), and is active on days with mean temperature between -5 and 10 ℃. The rate of chilling can be expressed as follows:

$$R_C = \begin{cases} \dfrac{1}{1+e^{C_a(x-C_c)^2+C_b(x-C_c)}} & if\ -5 \leq x \leq 10 \\ 0 & if\ x > 10\ or\ x < -5 \end{cases} \tag{1}$$

135   where x is the daily mean air temperature, and C_a, C_b, and C_c are chilling rate parameters.

The chilling phase ends with the onset of quiescence (t_1), which is when the state of chilling (S_C; Eq. 2) reaches the critical state of chilling (Eq. 3):

$$S_C = \sum_{t_0}^{t} R_C(x_t) \tag{2}$$

$$t = t_1\ \ if\ \ S_C > C^* \tag{3}$$

140   The forcing phase begins at t_1, and it is active on days with mean temperature is above 0 ℃.

$$R_F = \begin{cases} \dfrac{1}{1+e^{F_b(x-F_c)}} & if\ x > 0 \\ 0 & if\ x \leq 0 \end{cases} \tag{4}$$

where F_b and C_c are forcing rate parameters.

The forcing phase ends with the occurrence of SOS (t_2), which is when the state of forcing (S_F; Eq. 5) reaches the critical state of forcing (Eq. 6):

145
$$S_F = \sum_{t_1}^{t} R_F(x_t) \tag{5}$$

$$t = t_2 \quad if \quad S_F > F^* \tag{6}$$

The DM model (Delpierre et al., 2009) is based on the assumption that leaf senescence is driven both by the photoperiod and by low temperatures. This model represents the progress of senescence processes using a coloring state (S_{sen}) for each day (d), which is the accumulation of the daily rate of senescence (R_{sen}). Senescence starts on the date (D_{start}) when the photoperiod is

150
shorter than a certain threshold (P_{start}), and the EOS is recognized as when S_{sen} is larger than the threshold value Y_{crit}. The functions expressed in the process are as follows:

$$if \; P(d) < P_{start} \begin{cases} if \quad T(d) < T_b & R_{sen}(d) = [T_b - T(d)]^x \times f[P(d)]^y \\ if \quad T(d) \geq T_b & R_{sen}(d) = 0 \end{cases} \tag{7}$$

$$if \; \begin{cases} P(d) \geq P_{start} & S_{sen}(d) = 0 \\ P(d) < P_{start} & S_{sen}(d) = S_{sen}(d-1) + R_{sen}(d) \end{cases} \tag{8}$$

$$f[P(d)] = \frac{P(d)}{P_{strat}} \quad or \quad f[P(d)] = 1 - \frac{P(d)}{P_{strat}} \tag{9}$$

155
where $P(d)$ is the photoperiod on a given day d, $T(d)$ is the daily mean temperature (℃), and Tb is the critical temperature below which senescence processes are effective (℃).

We calibrated and validated the two phenology models using all pixel-year SOS and EOS data extracted from the GIMMS3g NDVI dataset during 1982–2018. Five phenological extraction methods (i.e., the HANTS-Maximum, Spline-Midpoint, Gaussian-Midpoint, Timesat-SG, and Polyfit-Maximum methods) were applied to obtain the mean phenological index value,

160
reducing the uncertainty caused by the use of only a single method (Fu et al., 2021). To match the spatial resolution of gridded meteorological data, the SOS and EOS data were resampled to 0.1° spatial resolution, and outliers were removed using the interquartile range method (Cui et al., 2017). We optimized parameters of the UniChill model (i.e., C_a, C_b, C_c, F_b, C_c, C^*, and F^*) and the DM model (i.e., P_{start}, T_b, x, y, and Y_{crit}) for each valid pixel in upper reaches of the Jinsha River watershed, minimizing root mean square error (RMSE) through particle swarm optimization. Phenology data from odd-

165
numbered years were utilized for parameter optimization, and even-numbered years were used for validation.

The warming-up, calibration, and validation periods for the original and modified SWAT-Carbon models were set at 2005–2006, 2007–2011, and 2012–2014, respectively. The calibration of modified SWAT-Carbon model involved the following

Hydrology and
Earth System
Sciences
Discussions
EGU
Open Access

two steps, whereas that of original SWAT-Carbon model only employed the second step. 1) We optimized the 8 parameters (Table S1) that control the shape, magnitude, and temporal dynamics of the LAI for forest and grassland through particle
170 swarm optimization, to align the simulated LAI curves with the observed dynamic LAI. 10 particles with different initial velocities were generated through the Latin hypercube sampling method. The Nash–Sutcliffe efficiency (NSE) was used as the objective function to continuously update the parameters. Optimal parameter sets were determined when the objective function remained unchanged after 10 iterations. 2) We adjusted those parameters that control the hydrological processes using SWAT-CUP 2019 (https://swat.tamu.edu/software/swat-cup/) (Abbaspour, 2008). The Sequential Uncertainty Fitting
175 (Sufi-2) algorithm in SWAT-CUP was used for sensitivity analysis, uncertainty analysis, and parameter calibration (Arnold et al., 2012). Overall, 18 parameters (Table S2) were used for model calibration. These parameters were derived by combining the 14 most sensitive parameters selected from the pool of 22 parameters for each original and modified model.

2.4 Model Evaluation

The widely used coefficient of determination (R^2), NSE, and percent bias (PBIAS) were selected as metrics to evaluate the
180 performance of the model in simulating the LAI and runoff in our study area (Moriasi et al., 2007):

$$R^2 = \frac{\left(\sum_{i=1}^{n} \left(O_i - \overline{O} \right) \left(P_i - \overline{P} \right) \right)^2}{\sum_{i=1}^{n} \left(O_i - \overline{O} \right)^2 \sum_{i=1}^{n} \left(P_i - \overline{P} \right)^2} \tag{10}$$

$$NSE = 1 - \frac{\sum_{i=1}^{n} \left(O_i - P_i \right)^2}{\sum_{i=1}^{n} \left(O_i - \overline{O} \right)^2} \tag{11}$$

$$PBIAS = \frac{\overline{P} - \overline{O}}{\overline{O}} \times 100\% \tag{12}$$

where n is the number of observations; O_i and P_i are the observed and simulated values, respectively, at time i; and $\overline{O}$ and $\overline{P}$
185 represent the average of the observed and simulated values, respectively.


3 Results

3.1 Spatiotemporal Variations in Climate and Vegetation Phenology

There is notable spatiotemporal heterogeneity in the multiyear mean annual temperature and accumulated precipitation across the upper reaches of the Jinsha River watershed (Figure 2a and b). The mean annual temperature exhibits a gradual
190 increase from the upstream to the downstream areas. The annual accumulated precipitation is higher in the downstream

region compared to the upstream. In addition, the mean annual temperature and accumulated precipitation showed clear temporal trends during 1982-2018. The mean annual temperature significantly increased by 0.06 °C per year on average. The annual accumulated precipitation across the entire watershed increased by 2.64 mm per year, however, downstream regions exhibited a declining trend (Fig.2b). Over the past four decades, the upper reaches of the Jinsha River watershed have

195 showed a "warming–wetting" trend in the upstream area and a "warming–drying" trend in some downstream areas.

During 1982–2018, the multiyear mean SOS and EOS in the upper reaches of the Jinsha River watershed were 164 ± 12.16 and 298 ± 10.56, (Day of year, DoY), respectively (Figure 2c and 2d). The mean SOS initiated in early May upstream and early July downstream. The mean EOS occurred in early October upstream, one month earlier than downstream. The SOS advanced in 60.5% of the study area over the past four decades, primarily in the middle and upper reaches of the watershed

200 (-0.05 ± 0.13 days per year), while being delayed by 0.09 ± 0.30 days per year in the downstream area. During the study period, the EOS was delayed by 0.08 ± 0.27 days per year in the downstream area but advanced by -0.03 ± 0.14 days per year in the upstream area. This spatiotemporal heterogeneity of vegetation phenology further highlights the importance of incorporating vegetation dynamics into hydrological models.
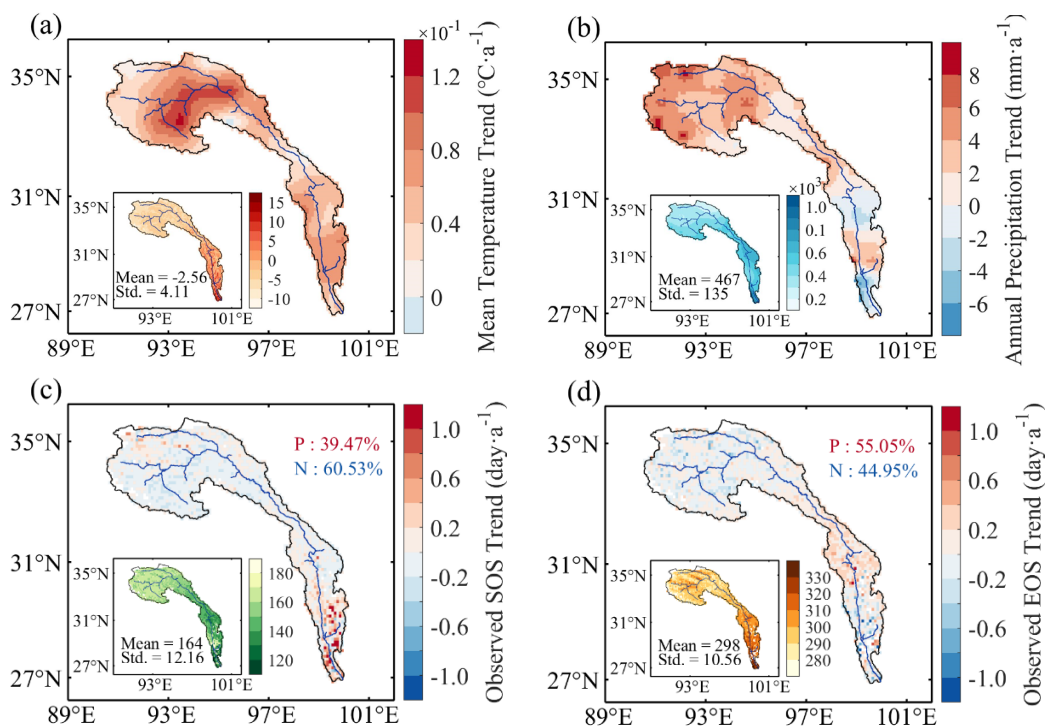
205 **Figure 2: Spatial and temporal variations of climatic variables and vegetation phenology during 1982–2018.** Temporal variations of mean annual temperature (a), accumulated annual precipitation (b), start-of-season (SOS, c) and end-of-season (EOS, d). The inner plot of each subfigure depicts the spatial pattern of the multi-year means of each variable.

3.2 Performance of Phenology Module and Modified SWAT-Carbon Model

The mean RMSE for the spring and autumn phenology models is 9.89 and 7.51 days, with calibration and validation RMSEs

210 of 8.71 and 10.82 days for SOS, and 7.03 and 7.77 days for EOS, respectively (Fig.3a and b). Within the study area, 67.1%
and 85.8% of pixels exhibited an RMSE of less than 10 days for SOS and EOS, respectively. The correlation coefficients
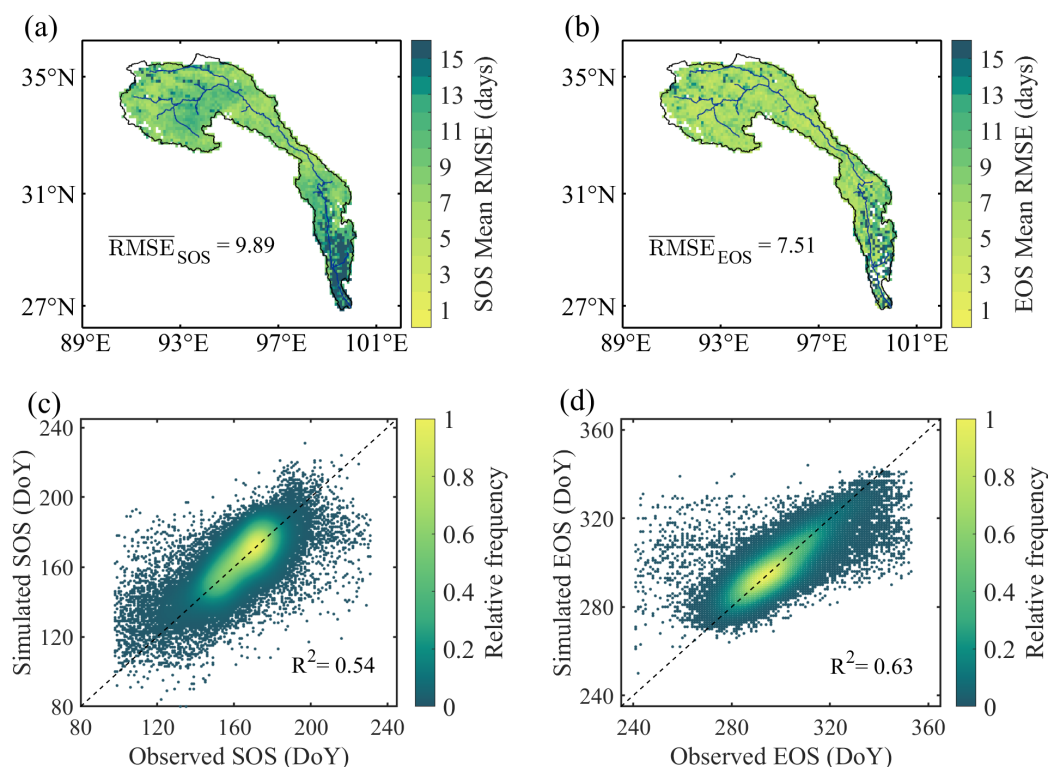between observed and simulated SOS and EOS are 0.54 and 0.63, respectively.

Figure 3: Performance of phenology module. Spatial patterns of the RMSE for start-of-season (SOS, a) and end-of-season (EOS, b).
215 Scatter plots depicting the relationship between simulated and observed start-of-season (SOS, c) and end-of-season (EOS, d). The colored
points on the scatter plots represent kernel density, with lighter colors indicating a higher density distribution. The dashed line represents
the 1:1 ratio line.

In the modified SWAT-Carbon model, the simulated LAI before the start of the growing season was changed to a non-zero

value for both the forest and grassland, and the calibrated and validated LAI growth curves largely improved compared to

220 the original model (Figure 4a and 4b, Table 2). Specifically, the average R^2 and NSE values improved from 0.31 and -1.42 to

0.79 and 0.78 for forest, and from 0.13 and -1.84 to 0.88 and 0.87 for grassland on average, respectively. Additionally, the

absolute PBIAS decreased by 41.0% for forest and 97.0% for grassland.

Incorporating phenology module into the SWAT-Carbon model enhanced the performance of runoff simulation. The

modified SWAT-Carbon model produced runoff simulations with a 'very good' level of performance ($0.80 < R^2 \leq 1$ and 0.75

225 $< \text{NSE} \leq 1$, Figure 4c and Table 2). Furthermore, the performance of runoff simulation in various months exhibited improvement, particularly during vegetation greening period (June), senescence period (October), and the non-growing season (Table S3). Specifically, the R^2 and NSE values for runoff increased by 0.13 and 0.39 in June, respectively, by 0.30 and 0.46 in October. The NSE value for runoff from November of the previous year to May increased by 0.35.

Table 2: Evaluation indices of the original and modified SWAT-Carbon model in simulating LAI and runoff.

Variable	Evaluation indices	Calibration (2007–2011)		Validation (2012–2014)	
		Original	Modified	Original	Modified
LAI (forest)	R^2	0.28	0.77	0.33	0.80
	NSE	-1.47	0.76	-1.36	0.79
	PBIAS (%)	42.77	-1.50	41.75	1.12
LAI (grassland)	R^2	0.11	0.87	0.15	0.89
	NSE	-1.87	0.86	-1.80	0.88
	PBIAS (%)	97.47	0.65	97.15	-0.01
Runoff	R^2	0.93	0.95	0.89	0.92
	NSE	0.92	0.95	0.86	0.92
	PBIAS (%)	4.80	1.75	5.04	1.22

230 R^2, coefficient of determination; NSE, Nash–Sutcliffe efficiency; PBIAS, percent bias.
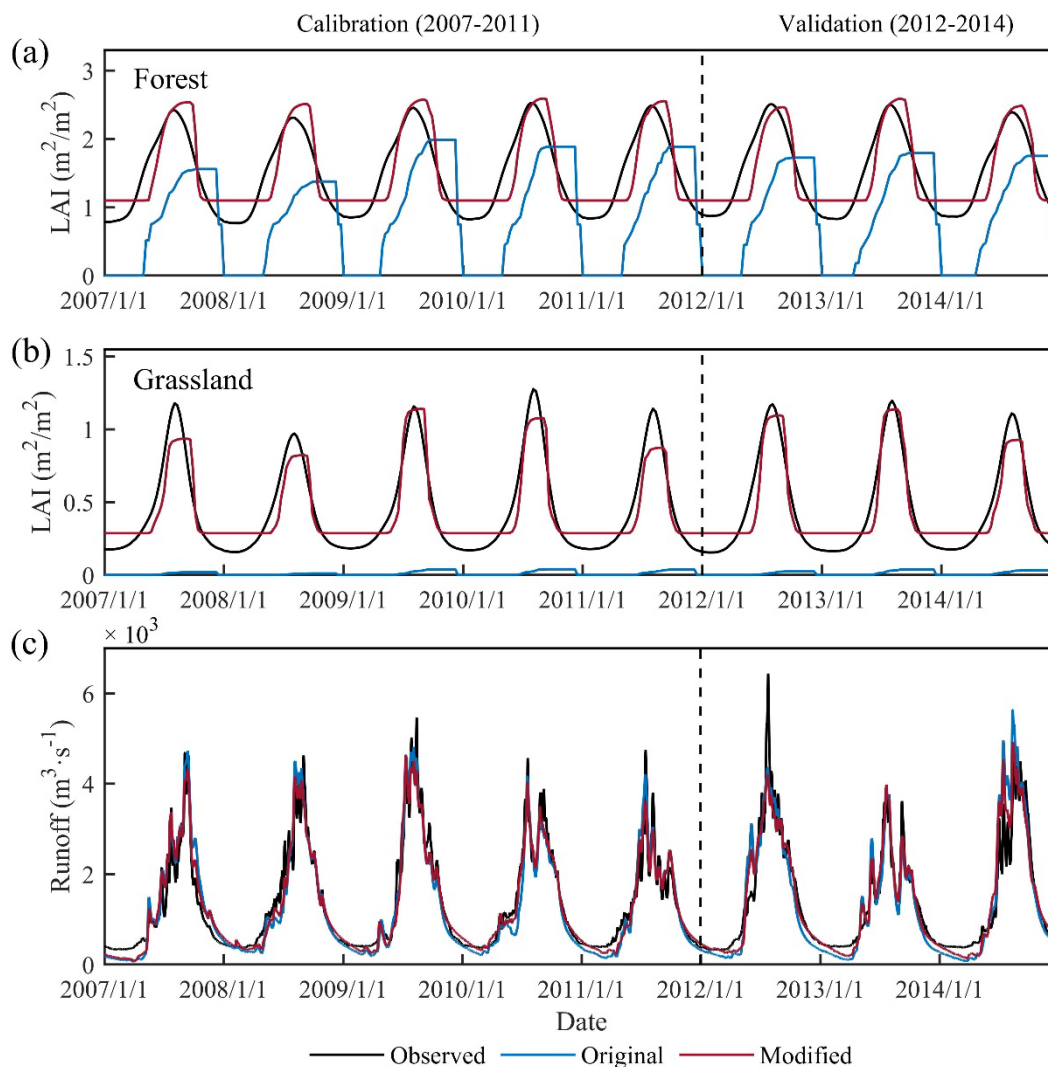
Figure 4: Temporal variability of the LAI and runoff during the calibration (2007–2011) and validation (2012–2014) periods. 8-d LAI time series observed by satellite and simulated by the original and modified SWAT-Carbon models for Forest (a) and grassland (b). Observed and simulated daily runoff by the original and modified SWAT-Carbon models (c).

3.3 Future Shifts in Vegetation Phenology and Runoff

The Unichill and DM phenology models were used to forecast future shifts in SOS and EOS during 2030–2100 under different emission scenarios. The SOS in the upper reaches of the Jinsha River watershed is projected to advance under all scenarios (Figure 5a), with the most significant advancement observed under the high-emission scenario (0.49 days per year, $p < 0.001$). In addition, a delaying trend in EOS was observed under all scenarios (Figure 5b), with the largest delay occurring under the high-emission scenario (0.18 days per year, $p < 0.001$).

Hydrology and
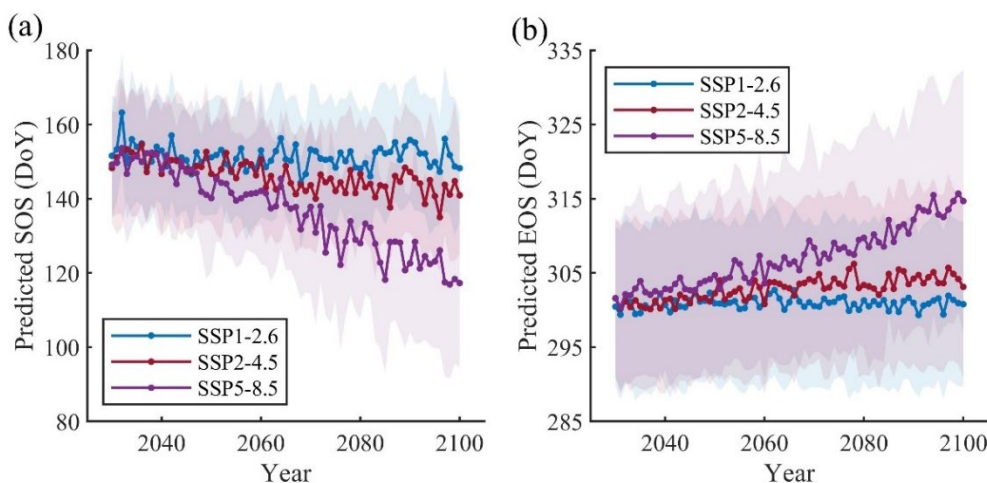Earth System
Sciences
Discussions
Open Access
EGU

Figure 5: Projection of future spring and autumn phenology during 2030–2100. Future shifts in start-of season (SOS, a) and end-of-season (EOS, b) under three Shared Socioeconomic Pathway (SSP) scenarios based on the Coupled Model Intercomparison Project Phase 6 (CMIP6) multi-model ensemble. SSP1-2.6, SSP2-4.5 and SSP5-5.8 refer to low, moderate and high emissions, respectively. Colored lines and shading represent the mean and one standard deviation, across the four CMIP6 models under each emission scenario.

The runoff under SSP5-5.8 exhibited greater fluctuation with continuous increase from 2023 to 2100. Specifically, runoff is projected to increase from approximately 1,437 m^3 s^{-1} in 2030 to 3,638 m^3 s^{-1} in 2100. However, the runoff under SSP1-2.6 and SSP2-4.5 is projected to initially increase and then stabilize after 2060 (Figure 6). The average runoff under SSP5-8.5 (2,459 m^3 s^{-1}) is greater than that under SSP1-2.6 (2,180 m^3 s^{-1}) and SSP2-4.5 (2,120 m^3 s^{-1}). Results from the original SWAT-Carbon model underestimated the future increases in runoff compared to those produced by the modified SWAT-Carbon model (Figure S1).
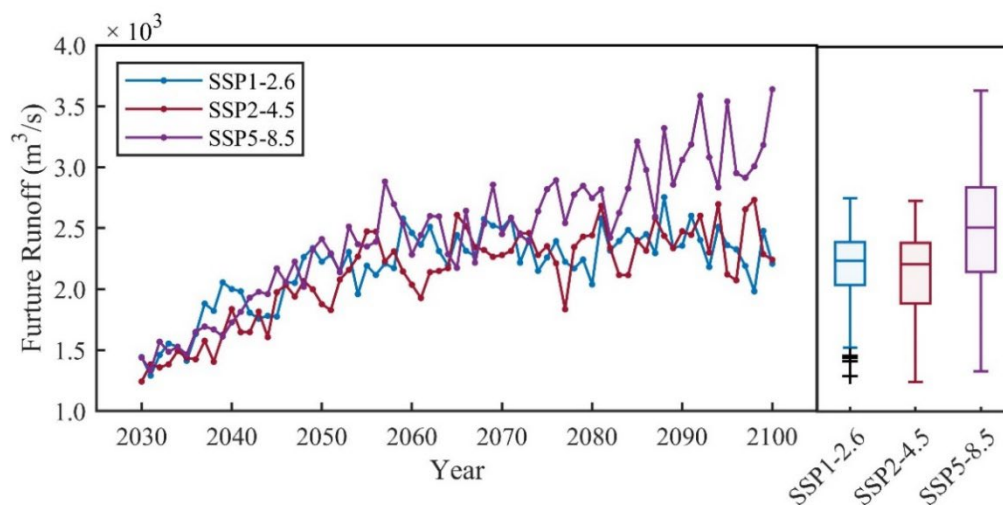

Figure 6: Projection of future runoff during 2030–2100 using the modified SWAT-Carbon model. The right subplot represents the annual mean runoff. SSP1-2.6, SSP2-4.5 and SSP5-5.8 refer to low emission, moderate and high emissions, respectively, based on the Coupled Model Intercomparison Project Phase 6 (CMIP6) multi-model ensemble.

Hydrology and
Earth System
Sciences
Discussions

Open Access

EGU

4 Discussion

4.1 Improvement of Runoff Simulation by Hydrological Model

Vegetation phenology has strong controls on seasonal and annual hydrological processes (Kim et al., 2018; Yang et al., 2023). During the start and end of the growing season, rapid changes in vegetation physiological properties such as stomatal

260 conductance and LAI influence the timing and amount of water resource allocation (Hwang et al., 2023; Zhang et al., 2021). Various environmental factors (e.g., temperature, precipitation, and radiation) and vegetation types determine the start and the end of the growing season (Wu et al., 2021), and process-based phenology models that incorporate different climatic factors have been well developed (Fu et al., 2020). However, the vegetation phenology in most hydrological models, such as the SWAT-Carbon model, is based on simple thermal and daylength thresholds (Arnold et al., 1998). This approach results

265 in larger uncertainty in vegetation dynamics and thereby hydrological processes predictions, especially under climate change (Zhang et al., 2009; Wang et al., 2022; Ma et al., 2019). In this study, we integrated process-based spring and autumn phenology models into the SWAT-Carbon model, which substantially improved the simulation of vegetation dynamics and ecohydrological processes, especially during the months of spring and autumn vegetation growth. Therefore, we highlight the importance of integrating a phenology module into hydrological models.

270 In addition to vegetation phenology, ecosystem structure, such as species composition is also affected by climate change (Chuine, 2010; Huang et al., 2019), which would substantially impact interactions between vegetation phenology and hydrology processes. Hence, more advanced land surface dynamic vegetation models, such as the LPJ-GUESS (Sitch et al., 2003), could be coupled with hydrological models to further improve our understanding of future vegetation dynamics and its effect on carbon and water cycles.

275 ### 4.2 Interaction between Vegetation Phenology and Hydrological Processes

Vegetation phenology and hydrological processes are closely intertwined through biotic and abiotic pathways (Buermann et al., 2018; Lian et al., 2020). For example, the physiological activity of vegetation and its impact on the underlying surface properties of a watershed affect land surface evapotranspiration (Chen et al., 2022b). In line with previous studies in the Northern Hemisphere, our study revealed a positive correlation between ET and growing season length, potentially attributed

280 to the prolonged period of water movement from the soil to the atmosphere (Geng et al., 2020; Yang et al., 2023). This was further verified by the observation that earlier leaf unfolding and delayed leaf senescence increased spring and autumn ET (Figure S2). Furthermore, vegetation phenology influences the development and decay of the canopy, altering the water demands of vegetation, and contributing to the augmentation of the water cycle (Hwang et al., 2018; Lian et al., 2020). However, our study found that both spring and autumn ET increased by a similar magnitude, with values of 1.58 and 1.62

285 mm per day, respectively. This finding is inconsistent with the asymmetrical increase reported in previous research (Kim et

al., 2018), which could be attributable to the abundant soil moisture during summer in our study area. This moisture abundance does not impose constraints on vegetation growth and transpiration.

The unrealistic representation of vegetation phenological processes in current hydrological models often requires remediation through additional ecohydrological processes (Luan et al., 2022), thereby compromising the fidelity mechanics.
290   For instance, calibration algorithms often lead to inaccurate representation of ecological processes despite producing accurate runoff simulations. Therefore, improving the simulation accuracy of vegetation dynamics could enhance the capability of hydrological models to accurately depict ecohydrological processes.

4.3 Hydrological Response to Future Climate Change and Vegetation Dynamics

We predicted future runoff in the upper reaches of the Jinsha River watershed under and found that the runoff would largely
295   increase under future emission scenario. Under the SSP5-8.5 scenario, runoff exhibited the most pronounced upward trend, primarily attributed to increased precipitation largely surpassing that of the SSP1-2.6 and SSP2-4.5 scenarios. In addition, despite a substantial increase in precipitation under SSP2-4.5 compared to SSP1-2.6, the projected runoff under SSP2-4.5 is marginally smaller than that under SSP1-2.6. This phenomenon can be attributed to the extension of the growing season under global warming, which would significantly increase evapotranspiration under the moderate emission pathway
300   compared to the low emission pathway (Lu et al., 2021; Yang et al., 2023). The increased precipitation under SSP2-4.5 is insufficient to fully counteract the increase in evapotranspiration caused by the prolonged growing season (Figure S3).

In summary, our study integrated a process-based vegetation phenology module into the SWAT-Carbon model, substantially improving the simulation of vegetation dynamics and hydrological processes in the upper reaches of the Jinsha River watershed. The runoff is predicted to increase over 2030-2100 under different future emission scenarios, primarily due to
305   greater precipitation outweighing the increase in evapotranspiration induced by the prolonged growing season. Our study highlights the importance of integrating phenological shifts into hydrological models. In the future, it will be crucial to consider and couple plant functional types into hydrological models to enhance the performance of ecohydrological process simulations. Furthermore, the phenology module should be incorporated into other hydrological models and applied in various watersheds to enhance our understanding of ecohydrological processes and to support future water resources
310   management under climate change conditions.

Data availability

Datasets for driving and evaluating the phenology models and the SWAT-Carbon model are available from the sources listed in Table 1.

Hydrology and
Earth System
Sciences
Discussions

Author contributions

315 Conceptualization: YF; Data curation: NW, JZ; Formal Analysis: ML, SC; Funding acquisition: YF, FH; Methodology: ML, SC, YX, ZW; Software: ML, SC; Supervision: YF; Validation: SC; Visualization: ML, JZ; Writing – original draft: ML; Writing – review & editing: SC, FH, NW, ZW, YX, JZ, YZ, YF.

Competing interests

The authors declare that they have no known competing financial interests or personal relationships that could have appeared
320 to influence the work reported in this paper.

Acknowledgments

325 **References**

Abbaspour K. C.: SWAT Calibration and Uncertainty Programs, 2008.

Arnold J. G., Srinivasan R., Muttiah R. S., and Williams J. R.: Large Area Hydrologic Modeling and Assessment Part I: Model Development, J. Am. Water Resour. As., 34, 73–89, https://doi.org/10.1111/j.1752-1688.1998.tb05961.x, 1998.

Arnold J. G., Moriasi D. N., Gassman P., Abbaspour K. C., White M. J., Srinivasan R., Santhi C., Harmel R. D., Van
330 Griensven A., Van Liew M. W., Kannan N., and Jha M. K.: SWAT: Model Use, Calibration, and Validation, T. ASABE, 55, 1491–1508, https://doi.org/10.13031/2013.42256, 2012.

Bhatta, B., Shrestha, S., Shrestha, P. K., and Talchabhadel, R.: Evaluation and application of a SWAT model to assess the climate change impact on the hydrology of the Himalayan River Basin, CATENA, 181, 104082, https://doi.org/10.1016/j.catena.2019.104082, 2019.

335 Bonan, G. B.: Forests and Climate Change: Forcings, Feedbacks, and the Climate Benefits of Forests, Science, 320, 1444–1449, https://doi.org/10.1126/science.1155121, 2008.

Buermann W., Forkel M., O'Sullivan M., Sitch S., Friedlingstein P., Haverd V., Jain A. K., Kato E., Kautz M., Lienert S., Lombardozzi D., Nabel J. E. M. S., Tian H., Wiltshire A. J., Zhu D., Smith W. K., and Richardson A. D.: Widespread seasonal compensation effects of spring warming on northern plant productivity, Nature, 562, 110–114,
340 https://doi.org/10.1038/s41586-018-0555-7, 2018.

Chen S., Fu Y. H., Geng X., Hao Z., Tang J., Zhang X., Xu Z., and Hao F.: Influences of Shifted Vegetation Phenology on Runoff Across a Hydroclimatic Gradient, Front. Plant Sci., 12, https://doi.org/10.3389/fpls.2021.802664，2022a.

Chen S., Fu Y. H., Hao F., Li X., Zhou S., Liu C., and Tang J.: Vegetation phenology and its ecohydrological implications from individual to global scales, Geography and Sustainability, 3, 334–338, https://doi.org/10.1016/j.geosus.2022.10.002, 2022b.

Chen S., Fu Y. H., Wu Z., Hao F., Hao Z., Guo Y., Geng X., Li X., Zhang X., Tang J., Singh V. P., and Zhang X.: Informing the SWAT model with remote sensing detected vegetation phenology for improved modeling of ecohydrological processes, J. Hydrol., 616, 128817, https://doi.org/10.1016/j.jhydrol.2022.128817, 2023.

Chuine, I.: A Unified Model for Budburst of Trees, J. Theor. Biol., 207, 337–347, https://doi.org/10.1006/jtbi.2000.2178, 2000.

Chuine, I.: Why does phenology drive species distribution?, Phil. Trans. R. Soc. B., 365, 3149–3160, https://doi.org/10.1098/rstb.2010.0142, 2010.

Creed, I. F., Hwang, T., Lutz, B., and Way, D.: Climate warming causes intensification of the hydrological cycle, resulting in changes to the vernal and autumnal windows in a northern temperate forest, Hydrol. Process., 29, 3519–3534, https://doi.org/10.1002/hyp.10450, 2015.

Cui T., Martz L., and Guo X.: Grassland Phenology Response to Drought in the Canadian Prairies, Remote Sens., 9, 1258, https://doi.org/10.3390/rs9121258, 2017.

Delpierre N., Dufrêne E., Soudani K., Ulrich E., Cecchini S., Boé J., and François C.: Modelling interannual and spatial variability of leaf senescence for three deciduous tree species in France, Agr. Forest Meteorol., 149, 938–948, https://doi.org/10.1016/j.agrformet.2008.11.014, 2009.

Fu, Y., Li, X., Zhou, X., Geng, X., Guo, Y., and Zhang, Y.: Progress in plant phenology modeling under global climate change, Sci. China Earth Sci., 63, 1237–1247, https://doi.org/10.1007/s11430-019-9622-2, 2020.

Fu Y. H., Campioli M., Demarée G., Deckmyn A., Hamdi R., Janssens I. A., and Deckmyn G.: Bayesian calibration of the Unified budburst model in six temperate tree species, Int. J. Biometeorol., 56, 153–164, https://doi.org/10.1007/s00484-011-0408-7, 2012.

Fu, Y. H., Piao, S., Op De Beeck, M., Cong, N., Zhao, H., Zhang, Y., Menzel, A., and Janssens, I. A.: Recent spring phenology shifts in western Central Europe based on multiscale observations, Global Ecol. Biogeogr., 23, 1255–1263, https://doi.org/10.1111/geb.12210, 2014.

Fu, Y. H., Zhao, H., Piao, S., Peaucelle, M., Peng, S., Zhou, G., Ciais, P., Huang, M., Menzel, A., Peñuelas, J., Song, Y., Vitasse, Y., Zeng, Z., and Janssens, I. A.: Declining global warming effects on the phenology of spring leaf unfolding, Nature, 526, 104–107, https://doi.org/10.1038/nature15402, 2015.

Fu, Y. H., Piao, S., Delpierre, N., Hao, F., Hänninen, H., Liu, Y., Sun, W., Janssens, I. A., and Campioli, M.: Larger temperature response of autumn leaf senescence than spring leaf-out phenology, Glob. Change Biol., 24, 2159–2168, https://doi.org/10.1111/gcb.14021, 2018.

375   Fu, Y. H., Zhou, X., Li, X., Zhang, Y., Geng, X., Hao, F., Zhang, X., Hanninen, H., Guo, Y., and De Boeck, H. J.:
          Decreasing control of precipitation on grassland spring phenology in temperate China, Global Ecol. Biogeogr., 30, 490–
          499, https://doi.org/10.1111/geb.13234, 2021.

        Gaertner, B. A., Zegre, N., Warner, T., Fernandez, R., He, Y., and Merriam, E. R.: Climate, forest growing season, and
          evapotranspiration changes in the central Appalachian Mountains, USA, Sci. Total Environ., 650, 1371–1381,
380   https://doi.org/10.1016/j.scitotenv.2018.09.129, 2019.

        Garonna I., de Jong R., and Schaepman M. E.: Variability and evolution of global land surface phenology over the past three
          decades (1982–2012), Glob. Change Biol., 22, 1456–1468, https://doi.org/10.1111/gcb.13168, 2016.

        Ge, Q., Wang, H., Rutishauser, T., and Dai, J.: Phenological response to climate change in China: a meta-analysis, Glob.
          Change Biol., 21, 265–274, https://doi.org/10.1111/gcb.12648, 2015.

385   Geng, X., Zhou, X., Yin, G., Hao, F., Zhang, X., Hao, Z., Singh, V. P., and Fu, Y. H.: Extended growing season reduced
          river runoff in Luanhe River basin, J. Hydrol., 582, 124538, https://doi.org/10.1016/j.jhydrol.2019.124538, 2020.

        Gudmundsson L., Bremnes J. B., Haugen J. E., and Engen-Skaugen T.: Technical Note: Downscaling RCM precipitation to
          the station scale using statistical transformations – a comparison of methods, Hydrol. Earth Syst. Sci., 16, 3383–
          3390, https://doi.org/10.5194/hess-16-3383-2012, 2012.

390   He, J., Yang, K., Tang, W., Lu, H., Qin, J., Chen, Y., and Li, X.: The first high-resolution meteorological forcing dataset for
          land process studies over China, Sci. Data, 7, 25, https://doi.org/10.1038/s41597-020-0369-y, 2020.

        Huang, M., Piao, S., Ciais, P., Peñuelas, J., Wang, X., Keenan, T. F., Peng, S., Berry, J. A., Wang, K., Mao, J., Alkama, R.,
          Cescatti, A., Cuntz, M., De Deurwaerder, H., Gao, M., He, Y., Liu, Y., Luo, Y., Myneni, R. B., Niu, S., Shi, X., Yuan,
          W., Verbeeck, H., Wang, T., Wu, J., and Janssens, I. A.: Air temperature optima of vegetation productivity across
395   global biomes, Nat. Ecol. Evol., 3, 772–779, https://doi.org/10.1038/s41559-019-0838-x, 2019.

        Hwang, T., Band, L. E., Miniat, C. F., Song, C., Bolstad, P. V., Vose, J. M., and Love, J. P.: Divergent phenological
          response to hydroclimate variability in forested mountain watersheds, Glob. Change Biol., 20, 2580–2595,
          https://doi.org/10.1111/gcb.12556, 2014.

        Hwang, T., Martin, K. L., Vose, J. M., Wear, D., Miles, B., Kim, Y., and Band, L. E.: Nonstationary Hydrologic Behavior in
400   Forested Watersheds Is Mediated by Climate-Induced Changes in Growing Season Length and Subsequent Vegetation
          Growth, Water Resour. Res., 54, 5359–5375, https://doi.org/10.1029/2017WR022279, 2018.

        Hwang T., Band L. E., Oishi A. C., and Kang H.: Greenup Variability Impact on Seasonal Streamflow and Soil Moisture
          Dynamics   in   Humid,   Temperate   Forests,   Water   Resour.   Res.,   59,   e2022WR034125,
          https://doi.org/10.1029/2022WR034125, 2023.

405   IPCC,2021: Climate Change 2021: The Physical Science Basis: Working Group I Contribution to the Sixth Assessment
          Report of the Intergovernmental Panel on Climate Change, Cambridge University Press, Cambridge, United Kingdom
          and New York, NY, USA, https://doi.org/10.1017/9781009157896, 2021.

Hydrology and
Earth System
Sciences
Discussions

Kim, J. H., Hwang, T., Yang, Y., Schaaf, C. L., Boose, E., and Munger, J. W.: Warming-Induced Earlier Greenup Leads to Reduced Stream Discharge in a Temperate Mixed Forest Catchment, J. Geophys. Res. Biogeo., 123, 1960–1975, https://doi.org/10.1029/2018JG004438, 2018.

410

Li, X., Long, D., Scanlon, B. R., Mann, M. E., Li, X., Tian, F., Sun, Z., and Wang, G.: Climate change threatens terrestrial water storage over the Tibetan Plateau, Nat. Clim. Change, 1–7, https://doi.org/10.1038/s41558-022-01443-0, 2022.

Lian, X., Piao, S., Li, L. Z. X., Li, Y., Huntingford, C., Ciais, P., Cescatti, A., Janssens, I. A., Peñuelas, J., Buermann, W., Chen, A., Li, X., Myneni, R. B., Wang, X., Wang, Y., Yang, Y., Zeng, Z., Zhang, Y., and McVicar, T. R.: Summer soil

415

drying exacerbated by earlier spring greening of northern vegetation, Sci. Adv., 6, eaax0255, https://doi.org/10.1126/sciadv.aax0255, 2020.

Lu J., Wang G., Li S., Feng A., Zhan M., Jiang T., Su B., and Wang Y.: Projected Land Evaporation and Its Response to Vegetation Greening Over China Under Multiple Scenarios in the CMIP6 Models, J. Geophys. Res. Biogeo., 126, e2021JG006327, https://doi.org/10.1029/2021JG006327, 2021.

420

Luan, J., Miao, P., Tian, X., Li, X., Ma, N., Abrar Faiz, M., Xu, Z., and Zhang, Y.: Estimating hydrological consequences of vegetation greening, J. Hydrol., 611, 128018, https://doi.org/10.1016/j.jhydrol.2022.128018, 2022.

Ma, T., Duan, Z., Li, R., and Song, X.: Enhancing SWAT with remotely sensed LAI for improved modelling of ecohydrological process in subtropics, J. Hydrol., 570, 802–815, https://doi.org/10.1016/j.jhydrol.2019.01.024, 2019.

Moriasi, D. N., Arnold, J. G., Liew, M. W. V., Bingner, R. L., Harmel, R. D., and Veith, T. L.: Model Evaluation Guidelines

425

for Systematic Quantification of Accuracy in Watershed Simulations, T. ASABE, 50, 885–900, https://doi.org/10.13031/2013.23153, 2007.

Mukundan, R., Gelda, R. K., Moknatian, M., Zhang, X., and Steenhuis, T. S.: Watershed scale modeling of Dissolved organic carbon export from variable source areas, J. Hydrol., 625, 130052, https://doi.org/10.1016/j.jhydrol.2023.130052, 2023.

430

Neitsch S. L., Arnold J. G., Kiniry J. R., and Williams J. R.: Soil and water assessment tool theoretical documentation version 2009, 2011.

Peñuelas J., Filella I., Zhang X., Llorens L., Ogaya R., Lloret F., Comas P., Estiarte M., and Terradas J.: Complex spatiotemporal phenological shifts as a response to rainfall changes, New Phytol., 161, 837–846, https://doi.org/10.1111/j.1469-8137.2004.01003.x, 2004.

435

Piao, S., Tan, J., Chen, A., Fu, Y. H., Ciais, P., Liu, Q., Janssens, I. A., Vicca, S., Zeng, Z., Jeong, S.-J., Li, Y., Myneni, R. B., Peng, S., Shen, M., and Peñuelas, J.: Leaf onset in the northern hemisphere triggered by daytime temperature, Nat. Commun., 6, 6911, https://doi.org/10.1038/ncomms7911, 2015.

Piao, S., Liu, Q., Chen, A., Janssens, I. A., Fu, Y., Dai, J., Liu, L., Lian, X., Shen, M., and Zhu, X.: Plant phenology and global climate change: Current progresses and challenges, Glob. Change Biol., 25, 1922–1940,

440

https://doi.org/10.1111/gcb.14619, 2019.

Shen, M., Wang, S., Jiang, N., Sun, J., Cao, R., Ling, X., Fang, B., Zhang, L., Zhang, L., Xu, X., Lv, W., Li, B., Sun, Q., Meng, F., Jiang, Y., Dorji, T., Fu, Y., Iler, A., Vitasse, Y., Steltzer, H., Ji, Z., Zhao, W., Piao, S., and Fu, B.: Plant phenology changes and drivers on the Qinghai–Tibetan Plateau, Nat. Rev. Earth Environ., 3, 633–651, https://doi.org/10.1038/s43017-022-00317-5, 2022.

445 Sitch S., Smith B., Prentice I. C., Arneth A., Bondeau A., Cramer W., Kaplan J. O., Levis S., Lucht W., Sykes M. T., Thonicke K., and Venevsky S.: Evaluation of ecosystem dynamics, plant geography and terrestrial carbon cycling in the LPJ dynamic global vegetation model, Glob. Change Biol., 9, 161–185, https://doi.org/10.1046/j.1365-2486.2003.00569.x, 2003.

Stevens B. and Bony S.: What Are Climate Models Missing?, Science, 340, 1053–1054,
450 https://doi.org/10.1126/science.1237554, 2013.

Strauch M. and Volk M.: SWAT plant growth modification for improved modeling of perennial vegetation in the tropics, Ecol. Model., 269, 98–112, https://doi.org/10.1016/j.ecolmodel.2013.08.013, 2013.

Thrasher B., Maurer E. P., McKellar C., and Duffy P. B.: Technical Note: Bias correcting climate model simulated daily temperature extremes with quantile mapping, Hydrol. Earth Syst. Sci., 16, 3309–3314, https://doi.org/10.5194/hess-16-
455 3309-2012, 2012.

Tian, P., Lu, H., Feng, W., Guan, Y., and Xue, Y.: Large decrease in streamflow and sediment load of Qinghai–Tibetan Plateau driven by future climate change: A case study in Lhasa River Basin, CATENA, 187, 104340, https://doi.org/10.1016/j.catena.2019.104340, 2020.

Vitasse, Y., Baumgarten, F., Zohner, C. M., Rutishauser, T., Pietragalla, B., Gehrig, R., Dai, J., Wang, H., Aono, Y., and
460 Sparks, T. H.: The great acceleration of plant phenological shifts, Nat. Clim. Change, 12, 300–302, https://doi.org/10.1038/s41558-022-01283-y, 2022.

Wang K., Onodera S., Saito M., Shimizu Y., and Iwata T.: Effects of forest growth in different vegetation communities on forest catchment water balance, Sci. Total Environ., 809, 151159, https://doi.org/10.1016/j.scitotenv.2021.151159, 2022.

Wilcke R. A. I., Mendlik T., and Gobiet A.: Multi-variable error correction of regional climate models, Climatic Change,
465 120, 871–887, https://doi.org/10.1007/s10584-013-0845-x, 2013.

Wu, Z., Chen, S., De Boeck, H. J., Stenseth, N. C., Tang, J., Vitasse, Y., Wang, S., Zohner, C., and Fu, Y. H.: Atmospheric brightening counteracts warming-induced delays in autumn phenology of temperate trees in Europe, Global Ecol. Biogeogr., 30, 2477–2487, https://doi.org/10.1111/geb.13404, 2021.

Wu Z., Fu Y. H., Crowther T. W., Wang S., Gong Y., Zhang J., Zhao Y.-P., Janssens I., Penuelas J., and Zohner C. M.:
470 Poleward shifts in the maximum of spring phenological responsiveness of Ginkgo biloba to temperature in China, New Phytol., 240, 1421–1432, https://doi.org/10.1111/nph.19229, 2023.

Yang Y., Roderick M. L., Guo H., Miralles D. G., Zhang L., Fatichi S., Luo X., Zhang Y., McVicar T. R., Tu Z., Keenan T. F., Fisher J. B., Gan R., Zhang X., Piao S., Zhang B., and Yang D.: Evapotranspiration on a greening Earth, Nat. Rev. Earth Environ., https://doi.org/10.1038/s43017-023-00464-3, 2023.

Hydrology and
Earth System
Sciences
Discussions

Open Access

EGU

475   Zhang H., Wang B., Liu D. L., Zhang M., Leslie L. M., and Yu Q.: Using an improved SWAT model to simulate hydrological responses to land use change: A case study of a catchment in tropical Australia, J. Hydrol., 585, 124822, https://doi.org/10.1016/j.jhydrol.2020.124822, 2020.

Zhang, X., Izaurralde, R. C., Arnold, J. G., Williams, J. R., and Srinivasan, R.: Modifying the Soil and Water Assessment Tool to simulate cropland carbon flux: Model development and initial evaluation, Sci. Total Environ., 463–464, 810–

480   822, https://doi.org/10.1016/j.scitotenv.2013.06.056, 2013.

Zhang X., Zhang Y., Ma N., Kong D., Tian J., Shao X., and Tang Q.: Greening-induced increase in evapotranspiration over Eurasia offset by CO_2-induced vegetational stomatal closure, Environ. Res. Lett., 16, 124008, https://doi.org/10.1088/1748-9326/ac3532, 2021.

Zhang Y., Chiew F. H. S., Zhang L., and Li H.: Use of Remotely Sensed Actual Evapotranspiration to Improve Rainfall–

485   Runoff Modeling in Southeast Australia, J. Hydrometeorol., 10, 969–980, https://doi.org/10.1175/2009JHM1061.1, 2009.

Zhao J., Zhang H., Zhang Z., Guo X., Li X., and Chen C.: Spatial and Temporal Changes in Vegetation Phenology at Middle and High Latitudes of the Northern Hemisphere over the Past Three Decades, Remote Sens., 7, 10973–10995, https://doi.org/10.3390/rs70810973, 2015.

490   Zhou S., Yu B., Lintner B. R., Findell K. L., and Zhang Y.: Projected increase in global runoff dominated by land surface changes, Nat. Clim. Change, 1–8, https://doi.org/10.1038/s41558-023-01659-8, 2023.